Title: CONVERGENCE AND ACCURACY OF KERNEL-BASED CONTINUUM SURFACE TENSION MODELS

CONF-9806154—

Author(s): M. W. Williams
D. B. Kothe
E. G. Puckett

Submitted to: Paper to be presented at the Chia-Shun Yia Memorial Symposium held at the 13th US National Congress of Applied Mechanics, June 21-26, 1998, Gainesville, FL

Los Alamos
NATIONAL LABORATORY

DISCLAIMER

DISCLAIMER

Portions of this document may be illegible in electronic image products. Images are produced from the best available original document.

Convergence and Accuracy of Kernel-Based Continuum Surface Tension Models *

M. W. Williams [†] D. B. Kothe [‡]

Los Alamos National Laboratory

Los Alamos, New Mexico, 87545

E. G. Puckett [§]

University of California, Davis

Davis, California, 95616

Abstract

Numerical models for flows of immiscible fluids bounded by topologically complex interfaces possessing surface tension inevitably start with an Eulerian formulation. Here the interface is represented as a color function that abruptly varies from one constant value to another through the interface. This "transition region", where the color function varies, is a thin $\mathcal{O}(h)$ band along the interface where surface tension forces are applied in continuum surface tension models. Although these models have been widely used since the introduction of the popular CSF method [BKZ92], properties such as absolute accuracy and uniform convergence are often not exhibited in interfacial flow simulations. These properties are necessary if surface tension-driven flows are to be reliably modeled, especially in three dimensions. Accuracy and convergence remain elusive because of difficulties in estimating first and second order spatial derivatives of color functions with abrupt transition regions. These derivatives are needed to approximate interface topology such as the unit normal and mean curvature. Modeling challenges are also presented when formulating the actual surface tension force and its local variation using numerical delta functions. In the following we introduce and incorporate kernels and convolution theory into continuum surface tension models. Here we convolve the discontinuous color function into a mollified function that can support accurate first and second order spatial derivatives. Design requirements for the convolution kernel and a new hybrid mix of convolution and discretization are discussed. The resulting improved estimates for interface topology, numerical delta functions, and surface force distribution are evidenced in an equilibrium static drop simulation where numerically-induced artificial "parasitic currents" are greatly mitigated.

1   INTRODUCTION

The central theme of continuum surface tension models is the formulation of surface tension effects as a localized *volumetric force*. This representation is quite different from earlier numerical models of interfacial phenomena, where surface tension is applied as a discrete boundary condition. In continuum models, surface tension acts on fluid elements everywhere within interface transition regions via the application of smoothly-varying forces. The integral effect of these forces recovers the surface tension boundary condition in the limit of an infinitely thin interface transition region. This basic formulation falls under the general class of immersed interface methods [LL94] whose origin dates back to the pioneering

work of Peskin [Pes77]. Continuum surface tension approaches are attractive when modeling topologically complex interfacial flows that experience merging and/or breakup. The challenge, however, is the development of continuum models that do not concede reductions in accuracy or convergence rate in return for the needed robustness. We strive to remove these concessions in this work.

In continuum surface tension formulations such as the CSF model, interfacial surface phenomena are replaced with smoothly varying volumetric forces derived by integrating surface tension forces per unit area over the interface surface. Surface tension is expressed as a volumetric force $\mathbf{F}_s$ satisfying

$$\mathbf{F}_s(\mathbf{x}_s) = \int_\Gamma \mathbf{f}_s(\mathbf{x})\delta(\mathbf{x} - \mathbf{x}_s)dS, \tag{1}$$

where $\mathbf{x}_s$ are points on the interface, Γ. The interface integral is over Γ, which is an arc length in two dimensions or a surface in three dimensions. The delta function is a product of one-dimensional delta functions (having units of inverse length):

$$\delta(\mathbf{x} - \mathbf{x}_s) = \prod_i \delta(x_i - x_{is}). \tag{2}$$

The surface tension force per unit interfacial area, $\mathbf{f}_s$, is given by [BKZ92]:

$$\mathbf{f}_s = \sigma\kappa\hat{\mathbf{n}} + \boldsymbol{\nabla}_s\sigma, \tag{3}$$

where σ is the surface tension coefficient, $\boldsymbol{\nabla}_s$ is the surface gradient [BKZ92], $\hat{\mathbf{n}}$ is the interface unit normal, and κ is the mean interfacial curvature, given by [Wea27]:

$$\kappa = -\boldsymbol{\nabla} \cdot \hat{\mathbf{n}}. \tag{4}$$

The first term in (3) is a force acting normal to the interface, proportional to the curvature κ. The second term is a force acting tangential to the interface toward regions of higher surface tension coefficient (σ). The normal force tends to smooth and propagate regions of high curvature, whereas the tangential force tends to force fluid along the interface toward regions of higher σ. Although σ does typically exhibit some dependence upon temperature and the presence of impurities (e.g., surfactants), we will assume σ to be constant in this work, hence neglect the tangential force.

In most Eulerian (fixed-grid) methods for interfacial flows, a color function C delineates the presence/absence of different fluids in the domain, hence C serves as a Heaviside function for some fluid. For this work, C is taken to be the fluid volume fractions f. The volume fractions f, while smoothly varying, nevertheless transition abruptly through the interface, hence estimating the first and second order spatial derivatives necessary for computing $\hat{\mathbf{n}}$ and κ is prone to noise and inaccuracies [BKZ92]. One solution is to first smooth f until its abrupt transition widens enough to support standard first and second order discretization stencils. In the original CSF model, volume fractions f are first convolved with a kernel K to yield a mollified function $\tilde{f}$. A quadratic B-spline was chosen for K in the CSF model [BKZ92], but this choice is by no means unique. Given the mollified function $\tilde{f}$, interface normals are computed in a straightforward manner,

$$\hat{\mathbf{n}} = \frac{\boldsymbol{\nabla}\tilde{f}}{|\boldsymbol{\nabla}\tilde{f}|}, \tag{5}$$

using standard forms for the discrete gradient operator. Once interface normals are obtained, curvatures follow easily from (4).

Since introduction of the CSF model, alternate kernels have been explored by others striving for higher fidelity estimates of interface normals n̂ and curvatures κ. Examples are the Gaussian kernel [Mon92], the cubic and quintic B-splines [Mort97, Rud98, Morr97], the Nordmark kernel [AP95], and the Peskin kernel [BMC97, BAM98]. Many of these same kernels are appropriate for discrete approximations to the surface integral in (1), where they represent smooth, finite-width Dirac delta functions (δ). Other notable approximations to δ are Peskin's cosine function [Pes77] and its subsequent modified forms that have been embraced in front tracking [JT97] and level set [SS97] methods.

We begin in Section 2 with a brief discussion of kernels and convolutions, after which we introduce a new kernel that has been specifically devised for continuum surface tension models. Next, in Section 3, we use this kernel and a hybrid mix of convolution and discretization techniques to demonstrate accuracy and high convergence rate for estimating curvatures along a simple interface. Finally, in Section 4, we test our new continuum model on an equilibrium static drop [BKZ92, KRM96], which is known to seed parasitic currents [LNS94] that can compromise solution quality. We conclude in Section 5 with suggestions for future work that will insure the necessary evolution of continuum surface tension models.

2   KERNELS AND CONVOLUTIONS

2.1   Convolution Model

In the convolution model, a discontinuous color function is convolved with a *kernel* (K) in order to smooth or "mollify" the discontinuities. In this work, the color function is represented by the volume fraction distribution f, but it could easily be the signed distance in level set methods, the phase field in phase field methods, or the indicator function in front tracking methods. The *convolution* of f with K at the point x, given by,

$$K * f(x) = \int_{\Omega} f(x')K(x' - x)dx' = \tilde{f}(x),$$ (6)

yields the mollified function $\tilde{f}(x)$.

The effect of a convolution is illustrated with the following 2-D example. Consider a circular drop, centered in a 4×4 domain, represented with a volume fraction field initialized to one and zero inside and outside the circle, respectively. For those cells containing the circular interface, f is set to a value between zero and one, in proportion to the cell volume truncated by the circle. The volume fraction field f, shown in Figure 1(a), undergoes a variation at the interface that is too abrupt for interface topology (n̂ and κ) discretizations to be reliable. If f is convolved, on the other hand, the resulting smooth approximation to the interface readily admits spatial derivatives. The convolved $\tilde{f}$, following the prescription in (6), yields a smooth volume fraction distribution, as shown in Figure 1b. The mollified transition region is now defined as those cells having a discrete $\tilde{f}$ between zero and one.

It is important to note that if K has continuous partial derivatives of all orders $n \le k$, then $\tilde{f}$ also has continuous partial derivatives of all orders $n \le k$, i.e., for any integer k, if
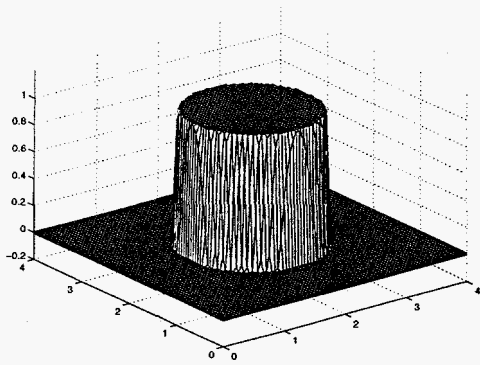
(a) Discontinuous color function, f **(b)** Convolved color function, $\tilde{f}$
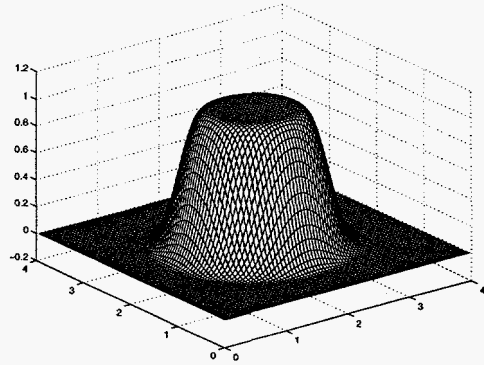
Figure 1: Discontinuous and convolved volume fractions for a unit circle on a 4×4 domain.

$K \in \mathcal{C}^k$ then $\tilde{f} \in \mathcal{C}^k$. In short, if K can be differentiated n times, then $\tilde{f} = K * f$ can also be differentiated n times, *even if f is a discontinuous function.*

In practice, there are a variety of ways to approximate the convolution integral. We currently approximate the convolution integral in (6) with a simple midpoint rule:

$$K * f(\boldsymbol{x}) = \int_{\Omega} K(\boldsymbol{x}' - \boldsymbol{x}) f(\boldsymbol{x}') \, d\boldsymbol{x}' \approx \sum_i K(\boldsymbol{x}'_i - \boldsymbol{x}) f(\boldsymbol{x}'_i) \, \Delta \boldsymbol{x}'_i. \tag{7}$$

A useful property common to all convolutions is that the derivatives of the convolution can be evaluated by simply convolving the scalar function with the differentiated kernel. For example, given $\boldsymbol{\alpha} = (\alpha_1, \alpha_2, \alpha_3)$, where each α_i is an integer, the spatial derivative of the convolved function $\tilde{f}$ is given by

$$\partial^{\boldsymbol{\alpha}} \tilde{f} = \partial^{\boldsymbol{\alpha}} (K * f) = (\partial^{\boldsymbol{\alpha}} K) * f = \int_{\Omega} f(\boldsymbol{x}') \partial^{\boldsymbol{\alpha}} K(\boldsymbol{x}' - \boldsymbol{x}) d\boldsymbol{x}',$$

$$\text{where } \partial^{\boldsymbol{\alpha}} = (\partial/\partial x_1)^{\alpha_1} (\partial/\partial x_2)^{\alpha_2} (\partial/\partial x_3)^{\alpha_3} = \prod_i (\partial/\partial x_i)^{\alpha_i}.$$

As an example, for $\boldsymbol{x} = (x, y, z)$ and $\boldsymbol{\alpha} = (1, 0, 0)$, the first derivative of the convolution with respect to x is given by

$$\frac{\partial \tilde{f}(\boldsymbol{x})}{\partial x} = \frac{\partial (K * f)}{\partial x}(\boldsymbol{x}) = (\frac{\partial K}{\partial x} * f)(\boldsymbol{x}) = \int_{\Omega} \frac{\partial K}{\partial x}(\boldsymbol{x}' - \boldsymbol{x}) f(\boldsymbol{x}') d\boldsymbol{x}'. \tag{8}$$

This operation will prove to be useful for estimating interface normals n̂, as shown later.

2.2   Choosing a Kernel

Choosing a kernel K that meets our design requirements is important for the practical use of convolutions in continuum surface tension modeling. Many types of kernels have been explored in the past, e.g., Gaussians, splines, smooth polynomials, cosine curves, etc. The portion of the domain over which the kernel is nonzero is called the *support* or *domain of dependence* of the kernel and is denoted by Ω_l. We let ϵ be representative of the support of the kernel, e.g., for a function with circular support, ϵ is the *radius of support*. Since the kernel is also a function of ϵ, we adopt the notation of $K(\boldsymbol{x}, \epsilon)$ for the kernel. For this work, we find that the kernel $K(\boldsymbol{x}, \epsilon)$ should

(a) $K_N(r, \epsilon = 0.4)$　　　　　　　　　**(b)** $K_8(r, \epsilon = 0.4)$
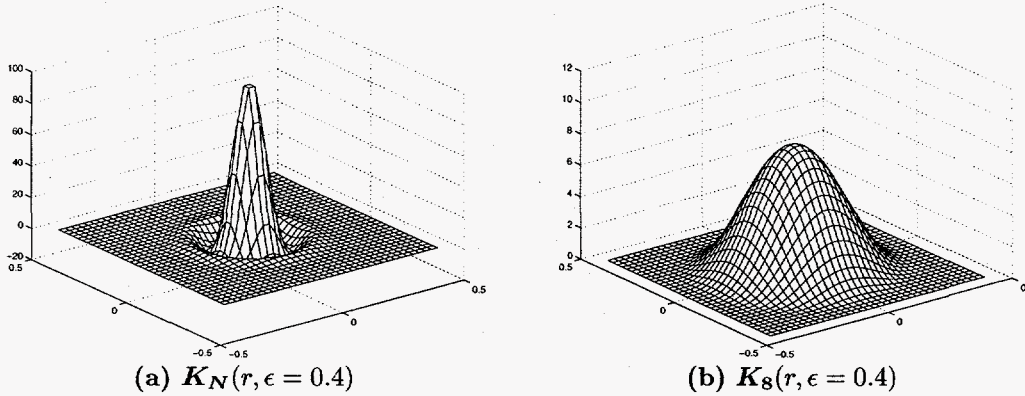
Figure 2: The Nordmark and eighth degree kernels on a unit domain.

(1) have compact support,

(2) be monotonically decreasing with respect to $|x|$,

(3) be smooth, i.e., for some $k \geq 1$, $K \in \mathcal{C}^k$,

(4) have a normality property, i.e., $\int_\Omega K(x, \epsilon) dx = 1$,

(5) and approach the Dirac delta function $\delta(x)$ in the limit $|\Omega_l| \to 0$.

Properties (1) and (2) are desired, but not required. For example, one may ignore (1) with a kernel having the entire domain Ω in its support (e.g., a Gaussian), but this tends to violate the locality associated with interfacial surface tension. Kernels that are non-monotonic, i.e., lacking property (2), tend to develop highly singular oscillations as $\Omega_l \to 0$. Kernel "smoothness", property (3), requires that the kernel be $\mathcal{C}^k$, as defined in Section 2.1. Properties (3) and (4) are necessary (but not sufficient) conditions for consistency and stability of the numerical convolution for a continuous function [AP95]. Property (5) is somewhat redundant, as it will always be satisfied if the first four properties are satisfied. It is not clear at this time if an additional radial symmetry property be required of the kernel, but all kernels we have studied to date are radially symmetric.

Two example kernels are illustrated in Figure 2, namely the Nordmark (K_N) kernel [Nor91] and a new eighth degree kernel (K_8). The K_8 kernel satisfies all properties above; K_N satisfies all but the monotonicity requirement, as is evident in Figure 2(a).

The K_8 kernel meets our design requirements (for $k = 3$), and has an additional advantage over several other kernels by virtue of its continuous third derivative. Its simple form is computationally efficient and trivial to implement, which is important since numerical integrations in multiple dimensions require many kernel evaluations. Our K_8 kernel is a monotonic eighth-degree polynomial function of the form:

$$K_8(r, \epsilon) = \begin{cases} A\left[1 - (r/\epsilon)^2\right]^4 & \text{if } r < \epsilon; \\ 0 & \text{otherwise,} \end{cases} \tag{9}$$

where A is a normalization constant that ensures $\int_\Omega K_8(r, \epsilon) dr = 1$. A plot of this kernel (for $\epsilon = 0.4$) is shown in Figure 2(b).

(a) $(\partial K_8/\partial x)(r, \epsilon = 1.00)$

(b) $(\partial^2 K_8/\partial x^2)(r, \epsilon = 1.00)$

(c) $(\partial K_8/\partial x)(r, \epsilon = 0.50)$

(d) $(\partial^2 K_8/\partial x^2)(r, \epsilon = 0.50)$

(e) $(\partial K_8/\partial x)(r, \epsilon = 0.25)$

(f) $(\partial^2 K_8/\partial x^2)(r, \epsilon = 0.25)$
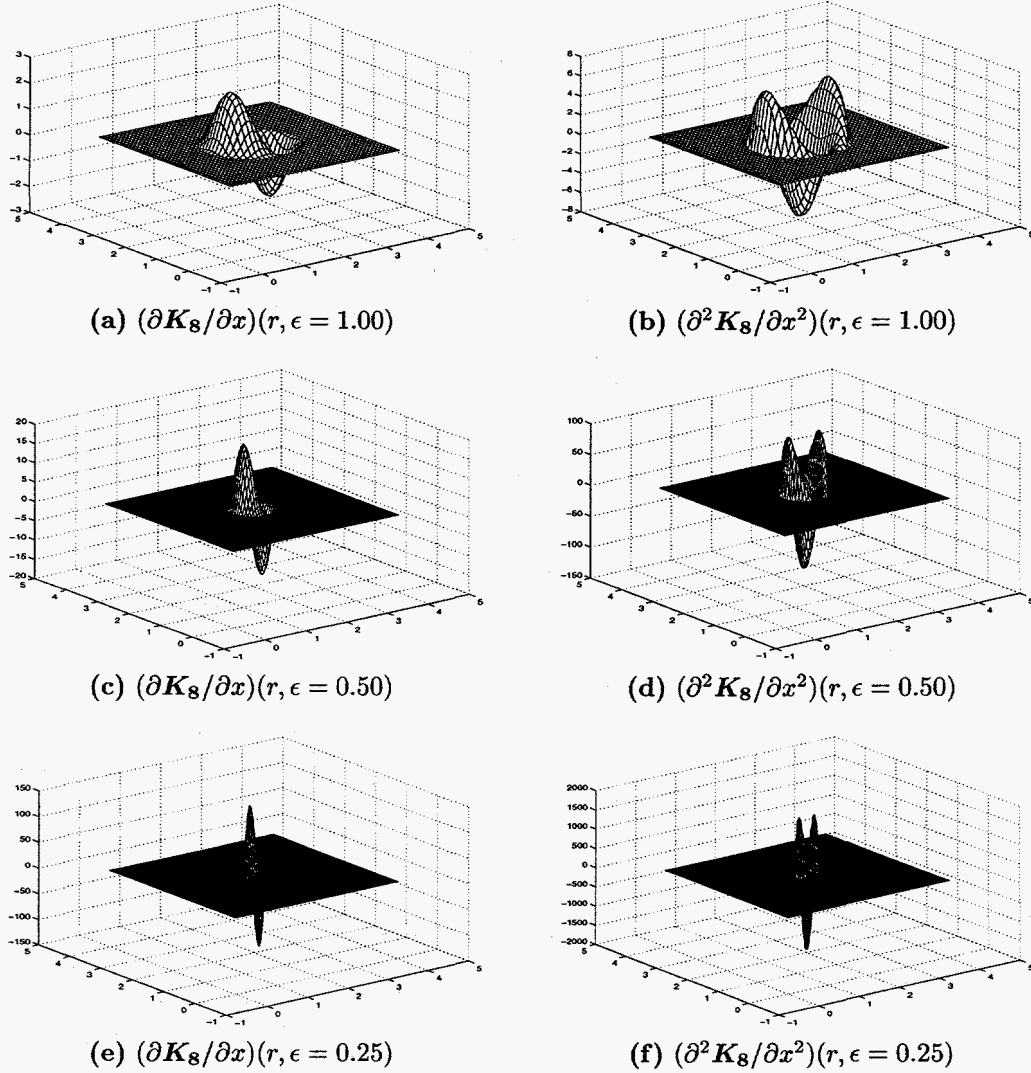
Figure 3: First and second derivatives of the K_8 kernel for different values of the support radius ϵ. A 4×4 domain is used with $\Delta x = \Delta y = \epsilon/10$.

2.3 Avoiding Singularities in the Kernel Derivatives

Figure 3 demonstrates another very important aspect of kernels. As $|\Omega_l| \to 0$, which corresponds to $\epsilon \to 0$, kernel derivatives tend to become singular. Resolving discontinuities and extrema in the kernel and its derivatives may require excessive numbers of discrete points within the kernel radius of support. For any given kernel, then, it is important to understand and quantify the relationship between the limits of $|\Omega_l| \to 0$ and $\Delta x \to 0$. For example, in Figure 3 it is apparent that second derivative extrema values are growing at a much faster rate than those for the first derivative (note the different plot scales). Growth of these singularities is even more severe for non-monotonic kernels. Any numerical convolution of second order and higher derivatives, therefore, requires many discrete points within $r < \epsilon$ to yield accurate approximations to the actual convolution. Table 1 provides evidence for this tendency, where discretization errors for the numerical second derivative convolution are quite large, even with many discrete points within the radius of support.

$\epsilon/\Delta x$	Value of Convolution	$(\partial K_8/\partial x) * f$	$(\partial K_8/\partial y) * f$	$(\partial^2 K_8/\partial x^2) * f$	$(\partial^2 K_8/\partial y^2) * f$
4	Analytic	-4.75514	-2.86529	16.5622	2.00181
	Numeric	-4.69157	-2.80470	12.4195	-0.97652
	%Error	1.337	2.114	25.013	-148.78
8	Analytic	-1.96967	-5.47108	-5.16573	-1.24848
	Numeric	-1.96178	-5.44712	-5.84872	-1.83220
	% Error	0.4006	0.4379	-13.222	-46.75
16	Analytic	4.03704	4.10382	2.29008	1.97206
	Numeric	4.03189	4.10329	2.24012	2.52696
	% Error	-0.1276	-0.0129	-2.182	28.14

Table 1: Discretization errors in the convolution integral, taken at the point of maximum error in the curvature approximation along a unit circle ($\epsilon = 0.2$).

3   DETERMINING INTERFACE TOPOLOGY

A color function distribution (e.g., volume fractions f) that possesses an abruptly-varying transition region presents challenges for accurate estimates of interface topology. As stated in Section 1, the original CSF approach for determining interface topology was to estimate $\hat{n}$ and κ with standard first and second order spatial discretization of the discrete convolved volume fractions $\tilde{f}$ [BKZ92]. While straightforward in practice, this approach is prone to inaccuracies, especially under mesh refinement, where convergence can be elusive [KRM96]. We have therefore pursued alternate approaches, which, similar to other recent works [Mort97, Rud98, Morr97, BMC97, BAM98], constitutes a *hybrid* method for estimating $\hat{n}$ and κ that involves both convolutions and standard discretization techniques.

In our hybrid prescription, consistently accurate and convergent estimates for κ are possible, following from (4), except that the interface normals used in (4) are *convolved* normals $\hat{n}$ resulting from convolution of f with the kernel first derivative as prescribed in (8). It is tempting to estimate curvatures via convolution of kernel *second* derivatives (as in [AP95]), but, as Table 1 shows, it is *very* difficult to estimate second derivative convolution integrals with an acceptable level of accuracy unless the support radius ϵ is at least an order of magnitude greater that Δx. As shown in Table 1, discretization errors for the second derivative convolution can be quite large, while errors associated with the first derivative convolution are only a fraction of a percent. Results in Table 1 also indicate that even for $\epsilon/\Delta x = 16$, second derivative convolutions are not well resolved. This is unacceptable for any reasonable implementation. For the same problem, $\epsilon/\Delta x = 4$ provides much more accurate approximations of the first derivative convolution. We feel this evidence justifies the approach of the hybrid method. In fact, the hybrid method has proven effective at predicting curvatures ranging over several orders of magnitude while using only $\epsilon/\Delta x = 4$.

In our hybrid method, convolved interface normals are computed with our K_8 kernel rather than the K_N kernel as proposed by Aleinov and Puckett [AP95]. This is principally because K_N is non-monotonic and highly peaked, therefore requiring large values of $\epsilon/\Delta x$. As mentioned in Section 2.2, K_8 meets all our kernel properties, and it also delivers a larger

Δx	$\epsilon/\Delta x$	L^∞ Errors	Convergence Rate
0.05000	8	0.897640E-02	
0.02500	16	0.160431E-02	2.484
0.01250	32	0.021017E-02	2.932
0.00625	64	0.003208E-02	2.712

Table 2: Unit circle curvature errors, using the hybrid method, where curvatures are estimated by discretizing normals that are convolved with $K_8(r, \epsilon = 0.4)$.

Δx	$\epsilon/\Delta x$	L^∞ Errors	Convergence Rate
0.05000	8	4.92363E-01	
0.02500	16	0.83809E-01	2.555
0.01250	32	0.06907E-01	3.601
0.00625	64	0.00735E-01	3.232

Table 3: Unit circle curvature errors, using the hybrid method, where curvatures are estimated by discretizing normals that are convolved with $K_N(r, \epsilon = 0.4)$.

effective smoothing radius since it approaches zero as $r \to \epsilon$ more slowly than other kernels such as K_N (see Figure 2). Examples of the performance of hybrid method are given in Tables 2 and 3, where curvature estimates of a unit circle on a 4×4 domain indicate that both absolute accuracy (L^∞ error) and high convergence rate are achievable. This is in contrast to the same hybrid method using K_N instead of K_8, where high convergence rates are possible, but not without unacceptably large absolute errors. The L^∞ errors in Table 3 are twenty to fifty times greater than those in Table 2.

4 SURFACE FORCE FORMULATION

4.1 The CSF Form

Perhaps more difficult than estimating interface topology is the formulation of the volumetric surface tension force $\mathbf{F}_s$. This requires a discrete approximation to the interface integral in (1), yielding a force $\mathbf{F}_s$ that smoothly varies through the defined interface transition region. The original CSF model postulated that $\mathbf{F}_s$ be expressed as

$$\mathbf{F}_s \approx \mathbf{f}_s \, \delta_\Gamma, \quad \text{where} \quad \delta_\Gamma = |\nabla \mathrm{f}|, \tag{10}$$

hence the discrete interface delta function δ_Γ approximates the interface integral as simply the gradient magnitude of the *unmollified* color function (volume fraction f). Here Γ denotes the interface region where $|\nabla f|$ is nonzero. $\widetilde{\Gamma}$ denotes the *mollified* transition region where $|\nabla \tilde{f}|$ and $\delta_{\widetilde{\Gamma}}$ are nonzero. Note that since $\Gamma \subset \widetilde{\Gamma}$, then $\delta_\Gamma \subset \delta_{\widetilde{\Gamma}}$.

In devising a surface force in the form of (10), an additional approximation is often made by further convolving the force $\mathbf{F}_s$, which (for constant σ) assumes one of two general forms:

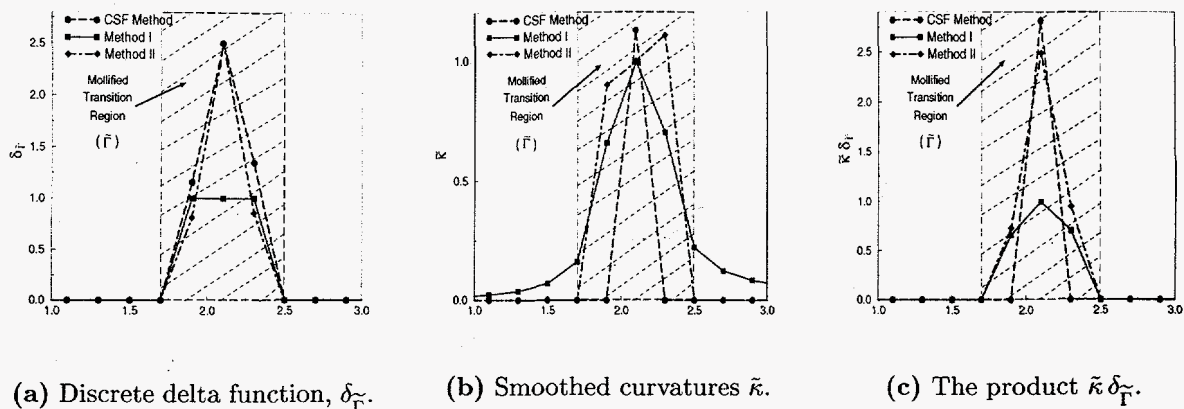$$\widetilde{\mathbf{F}}_s = \begin{cases} \widetilde{\mathbf{f}}_s \, \delta_\Gamma = \sigma \widetilde{\kappa} \hat{\mathbf{n}} \, \delta_\Gamma & \text{if } \kappa \text{ is smoothed}; \\[2mm] \widetilde{\mathbf{f}}_s \, \delta_{\widetilde{\Gamma}} = \sigma \widetilde{\kappa} \hat{\widetilde{\mathbf{n}}} \, \delta_{\widetilde{\Gamma}} & \text{if the transition region is also widened}. \end{cases} \tag{11}$$

Smoothing κ effectively defines curvatures off of the interface. These "off-interface" curvatures, denoted by $\tilde{\kappa}$, can be constructed in various ways. One can smooth the existing interface curvatures, κ, over any portion of the domain by convolving the interface curvatures with some kernel. Of course, the resulting distribution, $\tilde{\kappa}$, is very sensitive to the kernel choice. $\tilde{\kappa}$ can also be constructed by applying the same method used to estimate κ (e.g., our hybrid method) in $\tilde{\Gamma}$, the mollified transition region. If a convolution (or hybrid) method is used to estimate $\tilde{\kappa}$, the kernel radius of support (ϵ) should be several cells wider than the transition region, $\tilde{\Gamma}$. (For examples of $\tilde{\kappa}$ estimations via both approaches, see Figure 4(b).) In the first form for $\tilde{\mathbf{F}}_s$ above, surface forces still reside only within the transition region, Γ. In the second form, surface forces are applied throughout the mollified transition region through the application of $\delta_{\tilde{\Gamma}}$. Experience has shown, however, that convolved forces $\tilde{\mathbf{F}}_s$ must be used with caution, as too much (or incorrect) smoothing can violate the locality of surface tension and lead to erroneous surface pressures induced by the forces.

4.2   3-D Equilibrium Static Drop

A 3-D equilibrium static drop problem serves as an ideal test for the investigation of different surface force formulations. An 8^3 domain, partitioned with 40^3 cells, is occupied by two inviscid, incompressible fluids: a drop fluid and a background fluid. The drop fluid resides inside a spherical drop of radius $R = 2$ is centered in the domain. The background fluid, having one-tenth the drop density, occupies the remainder of the domain. Surface tension along the drop/background fluid interface is the sole force. The correct solution is a zero velocity field and a pressure field rising inside the drop to a value of $2\sigma/R = \sigma$. Computed velocity fields for three different force forms are shown in the vector plots of Figure 5. Results are shown for one and fifty computational time steps ($\delta t \approx 0.001$) in the xy-plane through the drop center.

The first force form follows the original CSF prescription, where surface forces $\mathbf{F}_s$ given by (10) are applied within the transition region, Γ. The other two forms invoke some smoothed force $\tilde{\mathbf{F}}_s$ applicable within the mollified transition region, $\tilde{\Gamma}$. For the CSF force, the discretization stencil used to determine $\delta_\Gamma = |\nabla f|$ results in a smooth function centered in the transition region, as seen in Figure 4(a). Note that in this case, δ_Γ remains nonzero within $\tilde{\Gamma}$ and not just Γ. For the method I force, curvatures κ are found only in Γ using the hybrid method described in Section 3. They are then convolved into a mollified $\tilde{\kappa}$ that enables curvatures to be defined throughout the wider $\tilde{\Gamma}$. The κ convolution, performed using a special singular kernel having infinite support, yields a $\tilde{\kappa}$ that varies smoothly from near zero at the edges of $\tilde{\Gamma}$ to a maximum value equal to the original κ at the interface, as shown in Figure 4(b). The $\delta_{\tilde{\Gamma}}$ used for method I is trivial: equal to unity inside $\tilde{\Gamma}$ and zero elsewhere, as shown in Figure 4(a). For the method II force, curvatures $\tilde{\kappa}$ throughout $\tilde{\Gamma}$ are found by directly applying the hybrid curvature method discussed in Section 3 to contours of f. In this case, $\tilde{\kappa}$ correctly exhibits the inverse radius dependence expected for a spherical interface, as seen in Figure 4(b). The $\delta_{\tilde{\Gamma}}$ used for method II is smoothly varying through $\tilde{\Gamma}$ and zero outside, attaining a maximum value along the actual interface, as shown in Figure 4(a). Given the forms chosen for the interface delta function and curvature, it is informative to examine the product $\tilde{\kappa} \delta_{\tilde{\Gamma}}$ in $\tilde{\Gamma}$, as shown Figure 4(c) for all three methods.

(a) Discrete delta function, $\delta_{\tilde{\Gamma}}$.   (b) Smoothed curvatures $\tilde{\kappa}$.   (c) The product $\tilde{\kappa}\,\delta_{\tilde{\Gamma}}$.

Figure 4: Three models for the variation of the interface delta function $\delta_{\tilde{\Gamma}}$, smoothed curvature $\tilde{\kappa}$, and their product $\delta_{\tilde{\Gamma}}\tilde{\kappa}$ through the mollified interface transition region $\tilde{\Gamma}$.
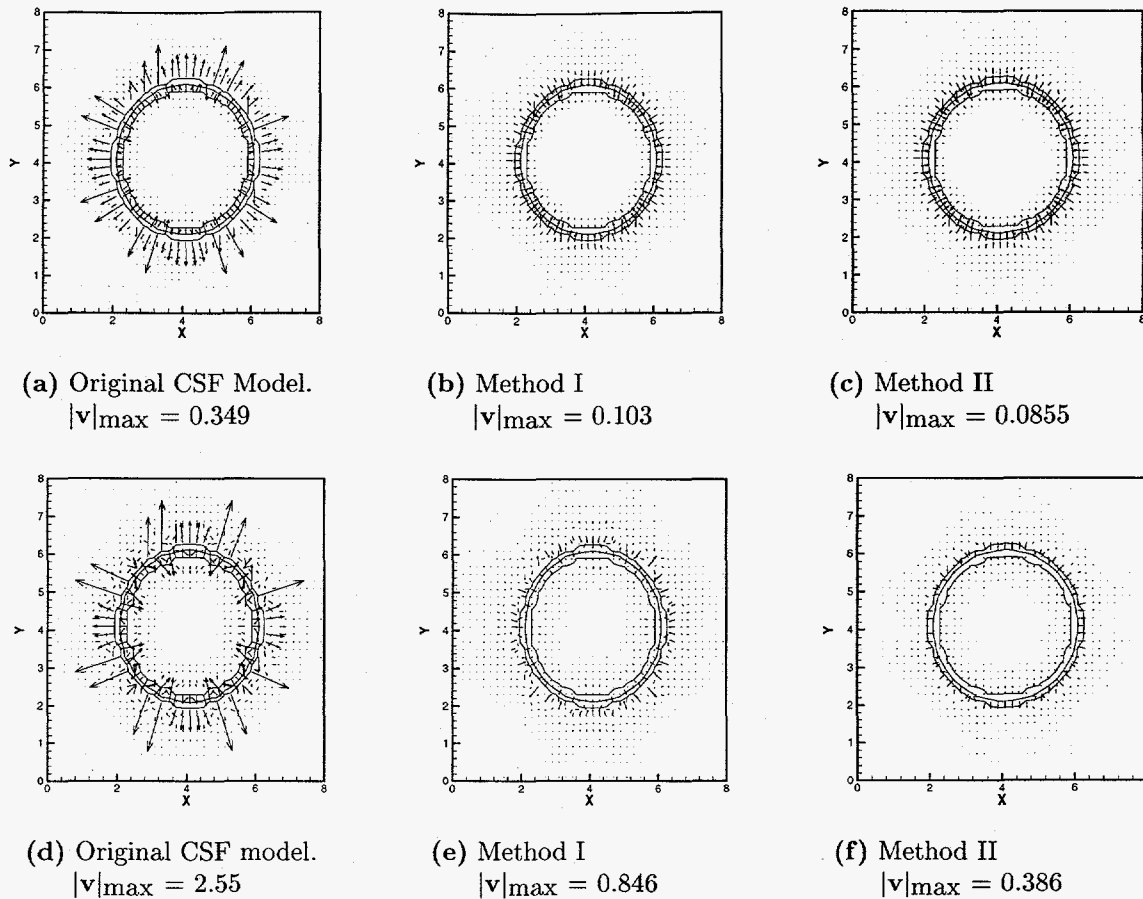
This variation shows how the surface force prescribed in either (10) or (11) is applied. As expected, the CSF force $\mathbf{F}_s$ is nonzero only within Γ, whereas the $\tilde{\mathbf{F}}_s$ forces are nonzero throughout the wider $\tilde{\Gamma}$ region.

It is evident in Figure 5 that both methods I and II reduce the static drop parasitic current strength (relative to the CSF model) by significant factors (three to five). Both the increased accuracy curvature estimates as well as a more smoothly-varying force $\tilde{\mathbf{F}}_s$ in a wider transition region $\tilde{\Gamma}$ are responsible for these improved results. It is not clear at this time, however, which effect is most important, but other verification measures such as reproducing the correct pressure jump will guide further model development. For this case, the CSF pressure jump errors (5%) are the smallest after one time step, but these errors grow with time (to 25% after 50 steps) because of the false flow dynamics, whereas the errors for methods I (40%) and II (20%) remain constant. We also plan to closely monitor the kinetic energy of this system, but non-solenoidal velocity filters for our colocated flow algorithm must be added before this data is meaningful [RKP98].

5   CONCLUSIONS AND SUMMARY

Despite the widespread use of continuum surface tension models in modeling surface tension effects along topologically complex interfaces, accuracy and convergence remain elusive. Convolution methods, on the other hand, especially those used in conjunction with standard discretization techniques, can greatly alleviate this problem. Accurate, high-order estimates of interfacial curvature are possible for convolution kernels that satisfy certain important design requirements. A new eighth-order order kernel K_8 satisfies these requirements, is easy to implement, and generates accurate results for acceptable ratios of support radius to mesh spacing. Convolution methods can also be applied to surface force distributions, yielding static drop results that represent a large improvement over the original CSF model.

Much algorithm work and model development remains, however. First, surface force forms resulting from a direct quadrature of the interface integral in (1) must be investigated [AP95, Rud98, BMC97]. Other so-called "reduced" force forms [SS97, RKP98] should

(a) Original CSF Model.
$|\mathbf{v}|_{\max} = 0.349$

(b) Method I
$|\mathbf{v}|_{\max} = 0.103$

(c) Method II
$|\mathbf{v}|_{\max} = 0.0855$

(d) Original CSF model.
$|\mathbf{v}|_{\max} = 2.55$

(e) Method I
$|\mathbf{v}|_{\max} = 0.846$

(f) Method II
$|\mathbf{v}|_{\max} = 0.386$

Figure 5: Velocity distributions in an xy plane through the drop center. Plots (a)–(c) are after one time step, $t = 0.001$, while plots (d)–(f) are after 50 time steps, $t \approx 0.05$.

also be investigated, as these forms result from energy considerations in which forces are estimated from the spatial gradients of surface free energies [Jac98]. Second, additional kernel properties such as variable support size and shape must be scrutinized. Third, the hybrid technique must be tested on more realistic interfaces having curvatures that vary rapidly along the interface (e.g., a sine curve). Finally, a systematic assessment of the impact of grid shape and mesh/interface orientation on accuracy and convergence is needed. These issues are currently under investigation.

References

[AP95]   I. Aleinov and E. G. Puckett. Computing surface tension with high-order kernels. In H. A. Dwyer, editor, *Proceedings of the Sixth International Symposium on Computational Fluid Dynamics*, pages 13–18, Lake Tahoe, NV, 1995.

[BAM98] M. Bussman, S. D. Aziz, J. Mostaghimi, and S. Chandra. Modeling the fingering of impacting droplets. Technical report, University of Toronto, Toronto, Canada, 1998. Submitted to *Physics of Fluids*.

[BKZ92] J. U. Brackbill, D. B. Kothe, and C. Zemach. A continuum method for modeling surface tension. *Journal of Computational Physics*, 100:335–354, 1992.

[BMC97]   M. Bussman, J. Mostaghimi, and S. Chandra. On a three-dimensional volume tracking model of droplet impact. Technical report, University of Toronto, Toronto, Canada, 1997. Submitted to *Physics of Fluids*.

[Jac98]   D. Jacqmin. A variational approach to deriving smeared interface surface tension models. In V. Venkatakrishnan, M. D. Salas, and S. R. Chakravarthy, editors, *Workshop on Barriers and Challenges in Computational Fluid Dynamics*, pages 231–240, Boston, MA, 1998. Kluwer Academic Publishers.

[JT97]   D. Juric and G. Tryggvason. Computations of boiling flows. Technical Report LA–UR–97–1145, Los Alamos National Laboratory, 1997. Accepted for publication in the *International Journal of Multiphase Flow*.

[KRM96]   D. B. Kothe, W. J. Rider, S. J. Mosso, J. S. Brock, and J. I. Hochstein. Volume tracking of interfaces having surface tension in two and three dimensions. Technical Report AIAA 96–0859, AIAA, 1996. [1] Presented at the 34rd Aerospace Sciences Meeting and Exhibit.

[LL94]   R. J. Leveque and Z. Li. The immersed interface method for elliptic equations with discontinuous coefficients and singular sources. *SIAM Journal on Numerical Analysis*, 31:1019–1044, 1994.

[LNS94]   B. Lafaurie, C. Nardone, R. Scardovelli, S. Zaleski, and G. Zanetti. Modelling merging and fragmentation in multiphase flows with SURFER. *Journal of Computational Physics*, 113:134–147, 1994.

[Mon92]   J. J. Monaghan. Smoothed particle hydrodynamics. *Annual Reviews in Astronomy and Astrophysics*, 30:543–574, 1992.

[Morr97]   J. P. Morris. Simulating surface tension with smoothed particle hydrodynamics. *International Journal for Numerical Methods in Fluids*, 1997. Submitted.

[Mort97]   D. E. Morton. *Numerical Simulation of an Impacting Drop*. PhD thesis, The University of Melbourne, Australia, 1997.

[Nor91]   H. O. Nordmark. Rezoning for higher order vortex methods. *Journal of Computational Physics*, 97:366–397, 1991.

[Pes77]   C. S. Peskin. Numerical analysis of blood flow in the heart. *Journal of Computational Physics*, 25:220–252, 1977.

[RKP98]   W. J. Rider, D. B. Kothe, E. G. Puckett, and I. D. Aleinov. Accurate and robust methods for variable density incompressible flows with discontinuities. In V. Venkatakrishnan, M. D. Salas, and S. R. Chakravarthy, editors, *Workshop on Barriers and Challenges in Computational Fluid Dynamics*, pages 213–230, Boston, MA, 1998.[1] Kluwer Academic Publishers.

[Rud98]   M. Rudman. A volume-tracking method for incompressible multifluid flows with large density variations. *International Journal for Numerical Methods in Fluids*, 1998. In Press.

[SS97]   M. Sussman and P. Smereka. Axisymmetric free boundary problems. *Journal of Fluid Mechanics*, 341:269–294, 1997.

[UT92]   S. O. Unverdi and G. Tryggvason. A front-tracking method for viscous, incompressible, multifluid flows. *Journal of Computational Physics*, 100:25–37, 1992.

[Wea27]   C. E. Weatherburn. On differential invariants in geometry of surfaces, with some applications to mathematical physics. *Quarterly Journal of Mathematics*, 50:230–269, 1927.

---

[1]Available at http://lune.mst.lanl.gov/Telluride/Text/publications.html.